Environmental Science & Technology

pubs.acs.org/est

Article

Stable Mercury Isotope Transition during Postdepositional Decomposition of Biomass in a Forest Ecosystem over Five Centuries

Wei Yuan, Xun Wang, Che-Jen Lin, Chuansheng Wu, Leiming Zhang, Bo Wang, Jonas Sommar, Zhiyun Lu, and Xinbin Feng*

Cite This: *Environ. Sci. Technol.* 2020, 54, 8739–8749

Read Online

ACCESS | Metrics & More | Article Recommendations | Supporting Information

ABSTRACT: Organic soil is an important transient reservoir of mercury (Hg) in terrestrial ecosystems, but the fate of deposited Hg in organic forest soil is poorly understood. To understand the dynamic changes of deposited Hg on forest floor, the composition of stable Hg and carbon (C) isotopes in decomposing litters and organic soil layer was measured to construct the 500 year history of postdepositional Hg transformation in a subtropical evergreen broad-leaf forest in Southwest China. Using the observational data and a multiprocess isotope model, the contributions of microbial reduction, photoreduction, and dark reduction mediated by organic matter to the isotopic transition were estimated. Microbial reduction and photoreduction play a dominant role in the initial litter decomposition during first 2 years. Dark redox reactions mediated by organic matter become the predominant process in the subsequent 420 years. After that, the values of Hg mass dependent fractionation (MDF), mass independent fractionation (MIF), and $\Delta^{199}Hg/\Delta^{201}Hg$ ratio do not change significantly, indicating sequestration and immobilization of Hg in soil. The linear correlations between the isotopic signatures of Hg and C suggest that postdepositional transformation of Hg is closely linked to the fate of natural organic matter (NOM). Our findings are consistent with the abiotic dark reduction driven by nuclear volume effect reported in boreal and tropical forests. We recommend that the dark reduction process be incorporated in future model assessment of the global Hg biogeochemical cycle.

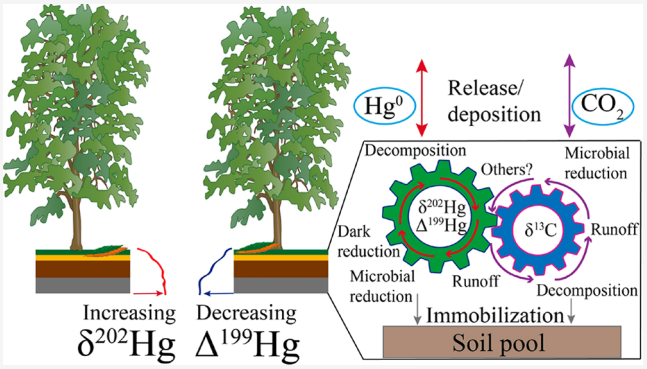

1. INTRODUCTION

Forest ecosystems represent an important sink of atmospheric gaseous elemental mercury (Hg^0).[1] Mercury (Hg) sequestered by litterfall is estimated to be 1000−1200 Mg yr^{-1} in global forest,[2,3] accounting for nearly 20% of total atmospheric Hg^0 burden (5000−5500 Mg).[4] Recent studies have established that Hg in forest soil is mainly derived from litterfall, instead of Hg wet deposition.[5−8] Soil is the largest carbon (C) and Hg reservoir in the terrestrial ecosystem.[8,9] Re-emission of Hg^0 and complexation of divalent mercury (Hg^{II}) take place simultaneously during litter degradation, while Hg tends to be accumulated in the remaining vegetative biomass.[10] Microbial reduction, photoreduction, and dark reduction are considered the primary processes facilitating the re-emission from forest soil.[7] In particular, dark redox reactions of Hg facilitated by natural organic matter (NOM), such as those observed in anoxic sediments and water,[11,12] have only recently been identified in forest soil.[7,13] Furthermore, previously deposited Hg in deeper organic soils (e.g., depth >5 cm) may not participate in the air−surface exchange processes extensively,[14,15] suggesting that the Hg accumulated in the soil pool.

Characteristics of Hg stable isotopes in environmental samples, quantified as mass dependent fractionation (MDF) and mass independent fractionation (MIF), provide a useful fingerprint for tracing Hg translocation and transformation in the environments.[16−18] Hg MDF (reported as $\delta^{202}Hg$) takes place in a wide variety of physical, chemical, and biological processes.[16,19−24] In contrast, only specific reactions can lead to Hg MIF (including odd-MIF reported as $\Delta^{199}Hg$ and $\Delta^{201}Hg$ and even-MIF reported as $\Delta^{200}Hg$ and $\Delta^{204}Hg$).[16,19,22−24] Processes causing odd-MIF include magnetic isotope effect (MIE) and nuclear volume effect (NVE). MIE can be triggered by photochemical (reduction) processes in aqueous solutions or snow crystals with $\Delta^{199}Hg/\Delta^{201}Hg$

Received: February 14, 2020
Revised: June 13, 2020
Accepted: June 17, 2020
Published: June 17, 2020

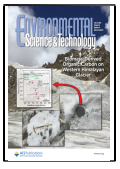

https://dx.doi.org/10.1021/acs.est.0c00950
Environ. Sci. Technol. 2020, 54, 8739−8749

ratios ranging from 1.0 to 1.2[25−28] and by methylmercury (MeHg) photodegradation with $\Delta^{199}Hg/\Delta^{201}Hg$ ratios in residual MeHg at ∼1.36.[25,29] NVE could be caused by equilibrium evaporation ($\Delta^{199}Hg/\Delta^{201}Hg$ slope = 1.59−2.00[23,30]), dark redox reactions mediated by organic matter ($\Delta^{199}Hg/\Delta^{201}Hg$ slope = ∼ 1.60[31,32]), photo oxidation processes ($\Delta^{199}Hg/\Delta^{201}Hg$ slope up to 1.89[33]), and self-shield in compact fluorescent lamps.[34] Even-MIF, with a slope of $\Delta^{200}Hg/\Delta^{204}Hg$ around −0.5, is caused by unidentified mechanisms in the atmosphere, most likely related to photochemical oxidation of Hg^0 exclusively in the upper atmosphere.[35]

Hg from various source components in forest ecosystems exhibits distinct odd-MIF signatures. For example, Hg in precipitation shows predominantly positive odd-MIF and even-MIF,[36,37] while Hg in vegetative biomasses shows significant negative odd-MIF but insignificant even-MIF.[1,5,7,36] In contrast, Hg in bedrock samples exhibits little odd-MIF and even-MIF.[16,38−40] Despite the increasing amount of data reported in the literature, there is a lack of knowledge in the interactions between the deposited Hg in the upper soil layer and the Hg retained in the deeper soil layer where Hg^{II} has been processed for centuries. Knowledge on the fate of Hg after deposition, such as transformation and translocation during biomass degradation, immobilization and sequestration in soil, re-emission to atmosphere, and runoff to downstream, is critical to the understanding of Hg cycling in forest ecosystems.

The objectives of this study are to understand the responsible sources and processes of vegetative biomass after deposition to the forest floor. We systematically observed the transition of Hg and C isotopic signatures in the samples of degrading biomass and organic soils in an attempt to understand the fate of deposited Hg on forest floor after active uptake by vegetation, as well as its association of C cycle, in an evergreen broad-leaf (EB) forest over a five-century period. The contribution of different biogeochemical processes to the isotopic shift during the biomass decomposition is determined using a stable isotope mass balance model. The transformation of mercury in aging organic soil is analyzed, and its implications on global mercury cycling are discussed.

2. MATERIALS AND METHODS

2.1. Site Description. The field work was performed at the Ailaoshan Station for Subtropical Forest Ecosystem Research Studies (ASSFERS, 24°32′ N, 101°01′ E, 2476 m elevation), Yunnan province, Southwest China. It has a subtropical climate with an annual mean temperature of 11.3 °C and precipitation depth of 1840 mm.[41] The canopy coverage is dominated by evergreen beech species (≥85%) with a stand age of >300 years; the detailed site information has been described in our earlier work.[42] Two experimental sites of 30 m × 30 m (A and B), 100 m apart, were set up for sampling (Figure S1). The undisturbed soil samples were collected at site A, and the litterfall decomposition experiments were performed at site B.

2.2. Soil Samples Collection and Litter Decomposition Experiment. The soil information and sampling operation are detailed in the Supporting Information (SI), Section 1. Briefly, three surface soil cores were randomly collected at 0−15 cm depth with overlaying litters at site A in January 2018. The soil profile was divided into the recent or slightly humified litter (horizon Oi), partially humified organic matter (horizon Oe), highly humified organic soil (horizon Oa), and mineral soil (horizon Ah, Figure S2). Because of the spatial heterogeneity, the soil horizon existed in a slight deviation. Layered soil samples with every 0.5 cm for the first 3 cm of soil column and every 1 cm for the rest 3−15 cm soil were dried, ground, and sieved with a 200-mesh nylon screen (74 μm) in sequence.

Litter decomposition experiments were performed according to the method described in our earlier work.[10] In summary, fresh litter samples were collected under the three dominant tree species (*Lithocarpus xylocarpus*, *Castanopsis wattii*, and *Schima noronhae*). The Hg concentration is consistent among different tree species,[10,43] and therefore, mixed composite samples were made for each experiment. Approximately 10.0 g of litter sample was placed in a 15 cm × 20 cm nylon bag with a 2 mm × 2 mm mesh size.[44] Twenty-four replicated nylon mesh bags divided into three groups were placed in three 1.0 m × 1.0 m ground cells under forest canopy at 2450 m above sea level at site B on August 31th, 2013. The sampling interval was every 2 months in the first year and every 4−8 months in the second year. The total decomposition period was 24 months. The decomposing samples were taken randomly in experimental plots and lightly rinsed by double distilled water (DDW) to remove surface soil and dust. The loss of Hg caused by the water rinse, assessed by exposing litter to water upon harvest, was negligible (<0.20 ng Hg g^{-1} dry mass), comparable to earlier results.[10,45] After carefully removing the impurities (roots and rubbles), the decomposed litterfall samples were dried at 60 °C for 72 h in an oven, followed by Hg, C, and stable isotopes analysis.

Total Hg concentration in soil and litter samples was measured by the Lumex Model RA-915+ (Lumex Analytics, detection limit: 1 ng g^{-1}) atomic absorption spectrometric analyzer at 254 nm with Zeeman correction for background absorption for interference-free measurement after combustion. The method recovery was determined to be 100.5 ± 2.5% (n = 9, mean = ±1σ) for soil samples using a certified soil reference material GBW07405 (290 ± 30 ng g^{-1}) and 96.2 ± 3.1% (n = 6, mean = ±1σ) for plant samples using a certified reference material GBW10020 (150 ± 20 ng g^{-1}).

2.3. Measurement of Hg and C Stable Isotopes. The measurement of Hg isotopes in composite litter and soil core samples has been described in our earlier work[8] and detailed in Section 2 of the SI. Mercury isotopic compositions were measured using a standard-sample-standard protocol and reported relative to NIST-3133 for MDF as follows:[25]

$$\delta^x Hg\ (‰) = \left[\frac{(^xHg/^{198}Hg)_{sample}}{(^xHg/^{198}Hg)_{NIST\text{-}3133}} - 1\right] \times 1000 \quad (1)$$

where x is the mass number of each Hg isotope from 199 to 202. MDF is reported as $\delta^{202}Hg$, and MIF is calculated as follows:[25]

$$\Delta^{199}Hg = \delta^{199}Hg - 0.2520 \times \delta^{202}Hg \quad (2)$$

$$\Delta^{200}Hg = \delta^{200}Hg - 0.5024 \times \delta^{202}Hg \quad (3)$$

$$\Delta^{201}Hg = \delta^{201}Hg - 0.7520 \times \delta^{202}Hg \quad (4)$$

The UM-Almadén standard was measured every 10 samples during measurement as a secondary standard. To ensure that the double-stage offline combustion-trapping technique (Hg recovery at 94.2 ± 1.5%) did not introduce discernible bias, BCR 482 and GSS-4 standards were measured before each

https://dx.doi.org/10.1021/acs.est.0c00950
Environ. Sci. Technol. 2020, 54, 8739−8749

analytical session. Results of UM-Almadén (δ^{202}Hg = −0.51 ± 0.04‰, Δ^{199}Hg = −0.01 ± 0.07‰, Δ^{200}Hg = 0.01 ± 0.06‰, Δ^{201}Hg = −0.01 ± 0.09‰, ± 2 SD, n = 7), BCR-482 (δ^{202}Hg = −1.56 ± 0.12‰, Δ^{199}Hg = −0.60 ± 0.06‰, Δ^{200}Hg = 0.06 ± 0.09‰, Δ^{201}Hg = −0.63 ± 0.02‰, ± 2 SD, n = 3), and GSS-4 (δ^{202}Hg = −1.72 ± 0.16‰, Δ^{199}Hg = −0.34 ± 0.06‰, Δ^{200}Hg = −0.00 ± 0.04‰, Δ^{201}Hg = −0.34 ± 0.06‰, ± 2 SD, n = 3) are consistent with the reported values.[25,46,47] Hence, we chose uncertainties of 0.12‰ for δ^{202}Hg, 0.07‰ for Δ^{199}Hg, 0.09‰ for Δ^{200}Hg, and 0.09‰ for Δ^{201}Hg (±2 SD) for the litter samples and 0.16‰ for δ^{202}Hg, 0.07‰ for Δ^{199}Hg, 0.09‰ for Δ^{200}Hg, and 0.09‰ for Δ^{201}Hg (±2 SD) for the soil profile samples.

Total organic carbon (TOC) concentrations were measured by a vario MACRO cube analyzer (Elementar, detection limit = 10 ppm). Carbon isotope measurements were accomplished by a Thermo-Fisher MAT 253 analyzer.[48] δ^{13}C was calculated as

$$\delta^{13}\mathrm{C}\ (‰) = 1000 \times [(^{13}\mathrm{C}/^{12}\mathrm{C}_{\mathrm{sample}})/(^{13}\mathrm{C}/^{12}\mathrm{C}_{\mathrm{V\text{-}PDB}}) - 1] \quad (5)$$

where Vienna Pee Dee Belemnite (V-PDB) was used as the δ-zero reference for C isotope measurement, and the mean δ^{13}C of IAEA-CH-3 standard substance was determined to be −24.716 ± 0.070‰ (n = 7, ± 2σ, recommended value = −24.724 ± 0.041‰).[10]

2.4. Radiocarbon Measurements. All soil samples were combusted, graphitized, and analyzed using accelerator mass spectrometry (AMS; National Electrostatics Corporation) at State Key Laboratory of Organic Geochemistry, Guangzhou, China. The ^{14}C results are reported as a fraction of modern ^{14}C (F^{14}C), after being corrected for mass fraction using δ^{13}C. The dating of soil age using ^{14}C data was calculated using published methods[49,50] with the Bacon Software package.[51] It is noted that the carbon in the soil samples represents a mixture of old and young carbon, i.e., the younger carbon could be introduced into the older soil by soil micro fauna activities and plant root exudate. Therefore, the interpretation of a bulk age should be used with caution.[7] The radiocarbon signal in the 0−5 cm soil samples resembles the signal of air samples in the present day.

2.5. Hg Isotopic Fractionation Model. It has been suggested that secondary processes do not induce Hg isotopic fractionation since desorbed Hg from soil or decomposing litter exists as Hg−NOM complexes.[52,53] Thus, the runoff process causes little Hg isotopic shift in residual Hg on the forest floor.[52] Geogenic Hg derived from weathering of bed rock has a greater (heavier) δ^{202}Hg (−0.68 ± 0.45‰, ± 1SD) than Hg on forest floor and exhibits little MIF of ^{199}Hg and ^{200}Hg.[16,38,54] We conclude that geogenic Hg is not an important Hg source in the 0−15 cm surface soil at the study site because of several observations. One is that ^{14}C dating results indicate that the soil profile is far younger than the rock, usually formed in a million year scale. The other is that Hg and C concentrations in 0−15 cm surface soil are 1 order of magnitude greater than those found in the deep soil and rock (Hg < 10 ng g^{-1} and C < 1%, respectively).[10] Although the C content decreases from 45% to 9% in from 1 to 15 cm depth soil, the level is still 1 order magnitude greater than the Hg level in deep mineral soil. Finally, observed Hg odd-MIF signatures decrease with the depth of soil. The trend does not support significant mixing of geogenic Hg in the soil layer, which would show positive Hg odd-MIF signatures.

Therefore, four governing processes were considered in modeling isotopic shift in the organic surface soil layer: microbial reduction, photoreduction (by organosulfur groups and DOM, respectively), and abiotic dark reduction mediated by NOM. The isotope mixing model was based on Hg isotope enrichment factor caused by Hg processes predicted by the Rayleigh equation to quantify the contribution of these processes. We used the Rayleigh equation to set up the model because of the following reasons. The Hg reduction and Hg^0 re-emission in forest floor to the atmosphere can be considered as loss of reaction products in an open system. It is also assumed that the Hg reduction processes are independent from each other. This is also verified with a model sensitivity analysis (Section 3.5). Finally, given the extensive Hg pool in soil compared to the Hg re-emission flux, we assume that each soil layer is relatively homogeneous. The Hg isotope mass model is built as follows and can be found in Section 3 of the SI:

$$f_{\mathrm{mic}} + f_{\mathrm{pho\text{-}S}} + f_{\mathrm{pho\text{-}C}} + f_{\mathrm{dar}} = 1 - F \quad (6)$$

$$\begin{aligned}&\varepsilon^{202}\mathrm{Hg}_{\mathrm{mic}} \times \ln(1 - f_{\mathrm{mic}}) + \varepsilon^{202}\mathrm{Hg}_{\mathrm{pho\text{-}S}} \times \ln(1 - f_{\mathrm{pho\text{-}S}}) \\ &\quad + \varepsilon^{202}\mathrm{Hg}_{\mathrm{pho\text{-}C}} \times \ln(1 - f_{\mathrm{pho\text{-}C}}) + \varepsilon^{202}\mathrm{Hg}_{\mathrm{dar}} \times \ln(1 - f_{\mathrm{dar}}) \\ &= \delta^{202}\mathrm{Hg}_{\mathrm{process}} - \frac{\delta^{202}\mathrm{Hg}_{\mathrm{initial}} + T \times \delta^{202}\mathrm{Hg}_{\mathrm{precipitation}}}{1 + T\ \%}\end{aligned} \quad (7)$$

$$\begin{aligned}&E^{199}\mathrm{Hg}_{\mathrm{mic}} \times \ln(1 - f_{\mathrm{mic}}) + E^{199}\mathrm{Hg}_{\mathrm{pho\text{-}S}} \times \ln(1 - f_{\mathrm{pho\text{-}S}}) \\ &\quad + E^{199}\mathrm{Hg}_{\mathrm{pho\text{-}C}} \times \ln(1 - f_{\mathrm{pho\text{-}C}}) + E^{199}\mathrm{Hg}_{\mathrm{dar}} \times \ln(1 - f_{\mathrm{dar}}) \\ &= \Delta^{199}\mathrm{Hg}_{\mathrm{process}} - \frac{\Delta^{199}\mathrm{Hg}_{\mathrm{initial}} + T \times \Delta^{199}\mathrm{Hg}_{\mathrm{precipitation}}}{1 + T}\end{aligned} \quad (8)$$

where f_{mic}, $f_{\mathrm{pho-S}}$, $f_{\mathrm{pho-C}}$, and f_{dar} are the fractional contribution of microbial reduction, organosulfur photoreduction, DOM photoreduction and NOM dark reduction, respectively. $\varepsilon^{202}\mathrm{Hg}_{\mathrm{mic}}$, $\varepsilon^{202}\mathrm{Hg}_{\mathrm{pho\text{-}S}}$, $\varepsilon^{202}\mathrm{Hg}_{\mathrm{pho\text{-}C}}$, and $\varepsilon^{202}\mathrm{Hg}_{\mathrm{dar}}$ are MDF enrichment factors caused by each of the four processes. $E^{199}\mathrm{Hg}_{\mathrm{mic}}$, $E^{199}\mathrm{Hg}_{\mathrm{pho\text{-}S}}$, $E^{199}\mathrm{Hg}_{\mathrm{pho\text{-}C}}$, and $E^{199}\mathrm{Hg}_{\mathrm{dar}}$ are odd-MIF enrichment factors caused by the respective processes, referring to the fraction of residual Hg, which means Hg remained in the soil without being involved in the reactions. $\Delta^{202}\mathrm{Hg}_{\mathrm{initial}}$ and $\Delta^{199}\mathrm{Hg}_{\mathrm{initial}}$ represent the Hg isotopic signatures in initial samples as Sp1 and So1, detailed in Tables S2 and S3. $\delta^{202}\mathrm{Hg}_{\mathrm{precipitation}}$ and $\Delta^{199}Hg_{\mathrm{precipitation}}$ represent the Hg isotopic signatures in precipitation.[55] T refers to the fractional contribution of Hg^{II} by precipitation mixed in the soil pool. Since throughfall Hg comes from rainfall Hg and additional Hg input during washout, it is assumed that the fraction of washed-out Hg contained in throughfall remains the in soil. Therefore, the products of T by throughfall Hg represent the amount of Hg retained in soil. The value of F in eq 6 is further estimated by

$$F = \frac{\mathrm{Hg}_i}{(t_i - t_{i-1}) \times (\mathrm{Hg}_{\mathrm{L}} + T \times \mathrm{Hg}_{\mathrm{T}})} \times 100\% \quad (9)$$

where t_i is the age for the i^{th} soil stage, Hg_i is the Hg mass retained in a given soil stage, Hg_{L} is the annual litterfall Hg deposition, and Hg_{T} is the annual throughfall Hg input. We assumed constant values for litterfall and throughfall Hg depositions during last 500 years on the basis of several reasons. One is that the variation of litterfall Hg deposition is

https://dx.doi.org/10.1021/acs.est.0c00950
Environ. Sci. Technol. 2020, 54, 8739−8749

mainly controlled by the litter biomass production since ASSFERS is a remote primordial forest with Hg^0 concentrations at 1.5−2.0 ng m^{-3}[56] without any deforestation or forest fires in last 500 years. The average precipitation Hg concentration is 4.9 ± 3.1 ng L^{-1} in the lower range observed at T/B forest sites in Europe and North America.[10] Therefore, the variation of throughfall Hg^{II} would not distinctly vary in last 500 years. Our earlier work suggested litterfall Hg deposition at ∼75 μg m^{-2} yr^{-1} and throughfall at ∼30 μg m^{-2} yr^{-1}.[10,43] The uncertainty associated with this assumption introduces immeasurable impact on our model results, especially in stage C with 420 year decomposition.

2.6. Sensitivity Analysis and Model Uncertainty. To explore the sensitivity of model response to the changes in fractionation parameters, the model results obtained by varying the input values of model parameters were compared using a two-level factorial design of experiment. The factorial design is meant to gauge the extreme variation caused by the possible range of all parameters. Data analysis of the factorial experiments was performed using Minitab 6.0. In short, values of model parameters were varied individually and in combinations at the two selected levels (i.e., a high and a low value). Then, the contribution of the reductive pathways (Table S4) at the changed input values was calculated and compared to estimate the sensitivity. The two-level factorial design of experiments provides an approximate estimate of model uncertainty. A Monte Carlo simulation was also performed to more accurately quantify the model uncertainties caused by model parameters. A 10 000 sample size of isotopic enrichment factors randomly ranging from the low level to the high level of Table S5 were selected for model simulation to estimate the range of contribution by different processes using eqs 6−9.

3. RESULTS AND DISCUSSION

The calibrated ^{14}C dating results suggest that the soil layer at 0−15 cm depth was formed in a 500 year period. On the basis of the observed Hg stable isotopes and the soil accumulation rate (Figure 1), the Hg biogeochemical processes in the soil profile can be divided into four stages. The first stage (∼2 years) is the initial decomposition of litter biomass, represented by surface litters decomposition bags experiments. The second stage (∼15 years) is the subsurface processes associated with continued litter decomposition, represented by 0−5 cm Oi and Oe soil horizons. In this stage, the soil samples show ^{14}C isotope characteristics similar to those found in present-day air samples. The third stage (∼400 years) is within the Oa soil horizon, represented by soil from 6 (dated as 17 ± 40 years old) to 11 cm (dated as 415 ± 60 years old) depth. The fourth stage is Hg immobilization in Ah soil horizons, represented by deeper soil from 11 (415 ± 60 years old) to 15 cm (486 ± 45 years old).

3.1. Hg Processes during the Initial Two Year Litter Decomposition. The litter decomposition experiment was designed to record the changes of concentration, mass, and isotopic signatures of Hg and C.[10] After two years of decomposition, the percentage of biomass loss is 61% ± 4% (n = 3) (Table S1), corresponding to a decrease from 45.9% to 31.5% for C content and an increase from 1.03% to 1.79% for N content. This yields a decrease in C/N ratios from 44.5 to 17.6 (Table S1 and Figure 2). Meanwhile, the Hg concentration increases from 97 ± 15 to 157 ± 13 ng g^{-1} with 26% ± 1% loss of total Hg mass after two years of

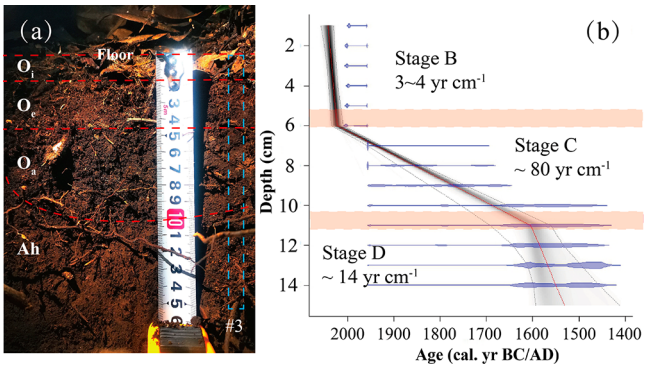

Figure 1. (a) Soil profile on forest floor down to 15 cm deep in present study. (b) Calculated soil age using radioactivity ^{14}C results[49,50] along the soil profile. The 0−5 cm soil profile represents stage B, which deposited during 2002−2018; the 5−11 cm soil profile represents stage C, which deposited during 1603−2012; the 11−15 cm soil profile represents stage D, which deposited during 1532−1603. The horizontal blue areas in (b) represent the calibrated ^{14}C dates (horizontal blue), the dark gray shadows indicate the more likely calendar ages, and gray stippled lines present the 95% confidence intervals; the red curve is the model 'best' estimated age. Only 14 cm yr^{-1} in stage D could be the result of a combination between soil compaction and gross matter deposition.

decomposition, suggesting relatively smaller Hg loss during the mineralization process (Table S2). During this period, $\delta^{202}Hg$ increases from −3.23 ± 0.12‰ to −2.93 ± 0.12‰ and $\Delta^{199}Hg$ decreases from −0.28 ± 0.07‰ to −0.34 ± 0.07‰. The MDF and odd-MIF shifts occur primarily during the second year (Figure 2c,d). Similar to the MDF change for Hg, $\delta^{13}C$ shows a small increase from −29.12 ± 0.07‰ to −28.69 ± 0.07‰ (Figure. 2g). The microorganisms responsible for litter decomposition preferentially consume lighter C, which therefore increases $\delta^{13}C$ in the decomposing litter.[57,58] However, this is balanced by the remaining lignin, which is recalcitrant to most soil bacteria and therefore exhibits a more negative $\delta^{13}C$.[57,58] Such a result is consistent with the earlier studies,[57,59] showing that litter bag decomposition experiments of up to five years cause insignificant $\delta^{13}C$ isotopic enrichment, even though the biomass loss can be as high as 69%.[57]

Manceau et al.[60] further showed that a substantial portion (up to 57%) of foliage bulk Hg^{II} consisted of precipitated nanoparticulate β-HgS at contaminated sites using X-ray absorption near-edge structure, suggesting a relatively inert state of this portion. After two years of litter decomposition, up to 74% of original Hg mass remains in the sample with >60% litter mass loss, also supporting that the inert Hg portion in litter is not readily reduced.[5,10] Our two year observation depicts that lighter isotopes appear to escape from decomposing litter with +0.30‰ shift in MDF (2 times of analytic uncertainty). In addition, the small negative shift of Hg odd-MIF in residual Hg^{II} of decomposing litter is only −0.06‰ after the two year period, comparable to the uncertainty level.

$\Delta^{200}Hg$ signatures in the samples remained relatively constant ($\Delta^{200}Hg$ = −0.04 ± 0.09, n = 8, ± 2σ), suggesting negligible contribution from precipitation Hg to the decomposition litters. The $\Delta^{200}Hg$ found in precipitation samples collected at ASSFERS is 0.23 ± 0.06‰ (±2σ),[55] consistent with the reported values in precipitation at remote sites (range, 0.08−1.18‰; mean, 0.25 ± 0.37‰; n = 47, ± 2σ).[36,37,61,62] The reactive Hg^{II} in precipitation reaching forest floor is

https://dx.doi.org/10.1021/acs.est.0c00950
Environ. Sci. Technol. 2020, 54, 8739−8749

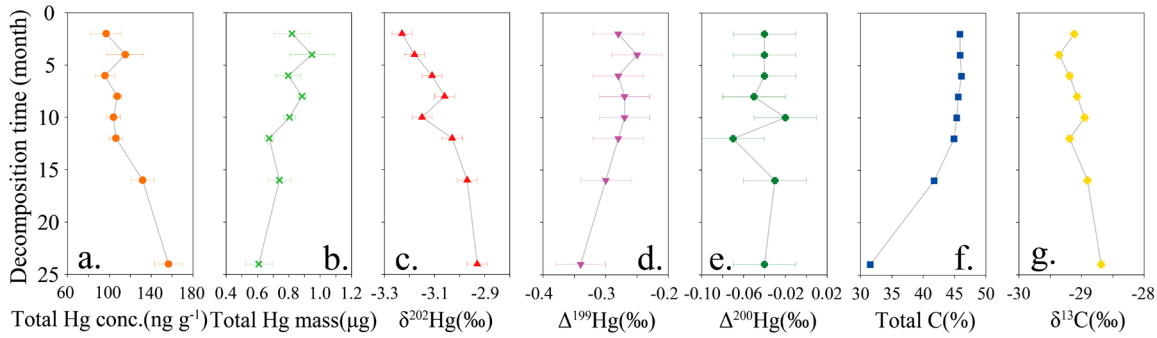

Figure 2. Temporal variation of the investigated variables with degradation time during the litter degradation experiments: (a) Hg concentration in residual litter, (b) total Hg mass in residual litter, (c) δ^{202}Hg in litterfall, (d) Δ^{199}Hg in litterfall, (e) Δ^{200}Hg in litterfall, (f) C concentration in litterfall, and (g) δ^{13}C in litterfall. The data points represent the mean of equal mass mixing of three experimental plots, except the total Hg concentration plot (a). Measurement error bars represent ±1 standard deviation.

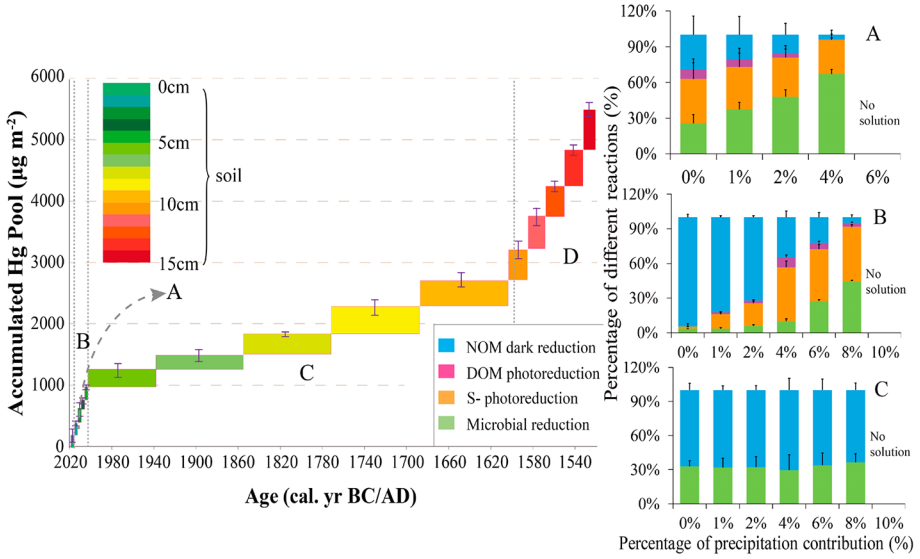

Figure 3. Evolution of accumulated Hg pool during postdepositional decomposition of litterfall along the soil profile in subtropical forest. The stages A–D represent the respective periods during postdepositional decomposition for 2 years, 20 years, 420 year, and 500 years. For stages A–C, the contributions from different reduction pathways were further calculated with various levels of precipitation Hg^{II} mixing.

possibly reduced to Hg^0 readily and re-emitted back to the atmosphere.[63] Another possibility is that the precipitation Hg^{II} is quickly transported to the downstream through runoff.

Given that precipitation mainly contains Hg^{II},[10] we estimated the contribution of Hg^{II} reduction pathways to the observed isotopic shifts in the litter samples under varying precipitation Hg^{II} during the two year decomposition period (Figure 3 and Figure S4). At 1% precipitation Hg^{II} mixed in forest floor, the contributions caused by microbial reduction, organosulfur-derived Hg^{II} photoreduction, photoreduction caused by DOM, and NOM dark reduction processes are 37 ± 6%, 36 ± 16%, 6 ± 5%, and 21 ± 15%, respectively. At 4% precipitation Hg^{II} input, the contributions from the above four pathways become 67 ± 4%, 29 ± 5%, 0 ± 1%, and 4 ± 4%, respectively. The increased contribution of microbial reduction with the elevated precipitation Hg^{II} input implies that the active Hg^{II} in wet deposition is expected to be preferentially reduced by microbes.[63] Further increasing the precipitation Hg^{II} input causes model divergence, suggesting that the precipitation Hg^{II} is <6%. This is consistent with model estimates using Δ^{200}Hg signature in air (mean: −0.05 ± 0.07‰, n = 33, ± 2σ)[42,64] and precipitation,[55] showing that 2–5% of Hg in decomposed litter comes from atmospheric Hg^{II} deposition. We highlight the importance of microbial reduction (48%~67%) and photoreduction (29%~37%) in the observed Hg loss during the two year litter decomposition, which is confirmed by ~1.0 slope of Δ^{199}Hg/Δ^{201}Hg in decomposing litter (Figure 4).

3.2. Hg Processes during the First 20 Years of Decomposition. With the continuous litterfall input, the aging litter biomass is gradually buried and compacted over time. In the 0–5 cm soil layer (deposited from 2002 to 2018), Hg concentration increases from 147 ± 1 to 190 ± 5 ng g^{-1} and then decreases to 177 ± 4 ng g^{-1} (Figure 5a and Table S3). The increasing soil bulk density with depth (from 802 to 1255 g m^{-2} cm^{-1}) offsets the decrease of soil Hg concentration (Figure S3), leading to a relatively constant soil Hg pool size of 143–205 μg m^{-2} cm^{-1}. The observed δ^{202}Hg gradually increases from −2.61 ± 0.16‰ in the topmost Oi soil to −2.13 ± 0.16‰ at 5 cm depth soil. In contrast, Δ^{199}Hg decreases from −0.44 ± 0.07‰ in topmost Oi soil to −0.53 ± 0.07‰ at 5 cm depth soil. The decrease trend is consistent with the observed C content (43.2%–20.3%), C/N ratio (21.38–16.09), and δ^{13}C shift (−29.02‰ to −27.28‰), respectively.

https://dx.doi.org/10.1021/acs.est.0c00950
Environ. Sci. Technol. 2020, 54, 8739–8749

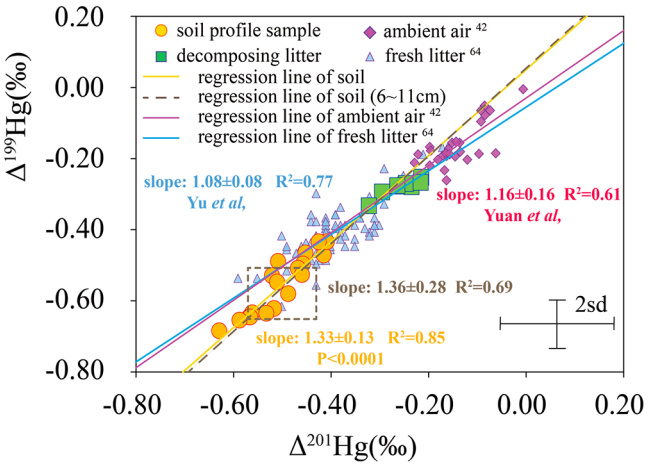

Figure 4. Scatter plots of Δ^{199}Hg versus Δ^{201}Hg in ambient air (pink filled diamonds),[42] fresh litter (blue filled triangle),[64] decomposing litter (green filled square), and soil profile (yellow filled circle) from present study. The yellow linear fit was obtained from Williamson−York bivariate regression method[65] using the soil samples. The gray dotted linear fit was obtained in only 6−11 cm soil results. The pink and blue linear fits were quoted from Yuan et al[42] for ambient air results and Yu et al.[64] for fresh litter results, respectively. The marked slopes are shown as mean ±1 standard deviation (SD). Measured error bar represents ±2 standard deviation.

During the 17 year deposition period, the Hg accumulation rate is ∼925 μg m^{-2}. We estimated 28%∼30% Hg loss from the original litters. Given the +0.48‰ δ^{202}Hg shift, the lighter Hg isotope is preferentially reacted in this decomposition stage. Assuming 1% contributions of Hg from precipitation (Figure 3 and Figure S4), the Hg loss caused by microbial reduction, photoreduction facilitated by organosulfur, photoreduction facilitated by DOM, and NOM dark reduction processes are 4 ± 4%, 13 ± 6%, 2 ± 2%, and 82 ± 5%, respectively. With 2%∼8% precipitation Hg^{II} input to soil Hg, the four pathways contribute to 6 ± 4%∼45 ± 3%, 20 ± 7%∼47 ± 14%, 2 ± 3%∼9 ± 7%, and 72 ± 5%∼5 ± 7% Hg loss in this soil profile, respectively. Compared to stage A during the first two years of decomposition, the fraction of photoreduction increases because of the longer period of exposure to sunlight, and the fraction of NOM dark reduction also increases because of the shading by subsequent litters.

3.3. Hg Dark Reduction Mediated by NOM in 20−420 Years of Soil Layer. During the period from 1603 to 2002 (corresponding to the 11−6 cm soil samples) with an average soil accumulation rate of ∼80 yr cm^{-1}, the soil bulk density increases from 1990 g m^{-2} cm^{-1} at 6 cm to 3917 g m^{-2} cm^{-1} at 11 cm due to soil compaction. The Hg concentration shows a relatively small increase from 102 ± 3 to 138 ± 1 ng g^{-1}. The Hg pool size also increases from 274 to 417 μg m^{-2} cm^{-1}. Given that the 5 cm soil shows δ^{202}Hg at −2.13 ± 0.16‰ and Δ^{199}Hg at −0.53 ± 0.07‰, there is a gradual positive shift (+0.34‰) in MDF and a −0.12‰ shift in odd-MIF at 11 cm depth (420 years old). The decreasing tendencies also occurred in the C content, C/N ratio, and δ^{13}C signature, with decreases at 9.2%, 15.59, and −26.48‰ (Table S3), respectively.

During this period (20−420 years), the Hg pool accumulated in this soil profile is ∼2200 μg m^{-2}, suggesting ∼93% Hg loss from the original litters. Assuming 1% contribution of Hg from precipitation (Figure 3 and Figure S4), the observed Hg loss caused by microbial reduction and NOM dark reduction is 33 ± 8% and 67 ± 4%, respectively. At elevated Hg^{II} input from wet deposition (2%∼8%), the contribution from the above two pathways becomes 30 ± 13%∼37 ± 11% and 63 ± 9%∼70 ± 12%, respectively. Compared to the earlier decomposition stages, the dark redox reactions induced by NOM are expected to play a more dominate role in Hg reductions in such soil layers,[7,32] which is also supported by observational evidence. The slope of Δ^{199}Hg/Δ^{201}Hg is a useful fingerprint to identify the geochemical processes,[16,35] since microbial reduction does not shift Hg odd-MIF.[20,21] The soil samples collected from the 0−15 cm soil profile show a Δ^{199}Hg/Δ^{201}Hg ratio of 1.33 ± 0.13 (mean ±1 SD, R^2 = 0.85, by Williamson−York regression,[65] $P < 0.0001$) (Figure 4). Especially, the slope of Δ^{199}Hg/Δ^{201}Hg obtained from the 6−11 cm soil samples is 1.36 ± 0.28. In addition, the linear regression of the Δ^{199}Hg versus δ^{202}Hg data exhibits a significant negative slope of −0.26 (−0.28 for all samples) (Figure S5), similar to those found in NOM-driven Hg^{II} dark reduction in soil with a slope of −0.24.[7,31] Moreover, the observed Δ^{199}Hg/Δ^{201}Hg ratio increases with increasing soil depth and reaches a maximum value (1.15−1.20) at the 420 year soil age (Figure S6). These findings suggest that nonphotochemical abiotic reduction of inorganic Hg^{II} by organic matters during pedogenesis is the most probable mechanism, followed by microbial reduction.

3.4. Hg Immobilization beyond 420 Year Soil Age. In the soil samples corresponding to the period from 1532 to

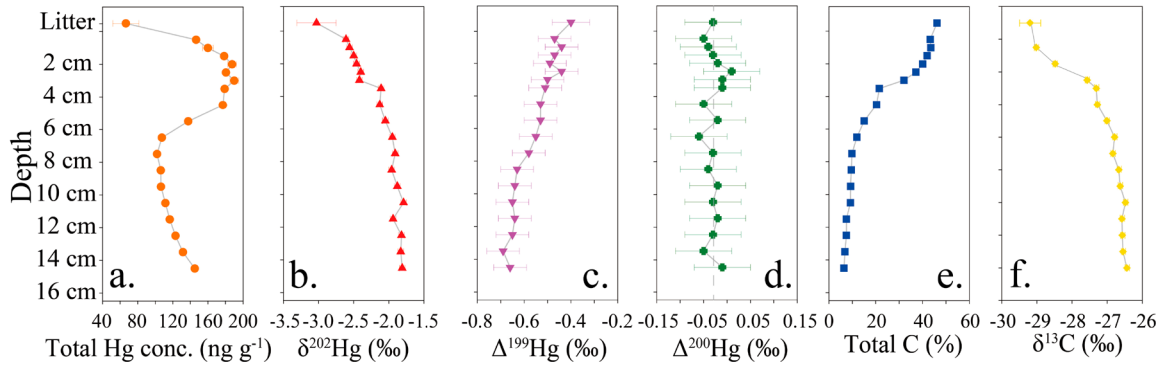

Figure 5. Vertical profiles of the investigated variables with soil depth in the undisturbed soil profile: (a) soil Hg concentration, (b) soil δ^{202}Hg, (c) soil Δ^{199}Hg, (d) soil Δ^{200}Hg, (e) soil C concentration, and (f) soil δ^{13}C. The litter represents the fresh litter on soil surface, which is from Yu et al.[64] The data points represent one experimental plot of #3. Measurement error bars represent ±1 standard deviation.

https://dx.doi.org/10.1021/acs.est.0c00950
Environ. Sci. Technol. 2020, 54, 8739−8749

1603 (15−11 cm soil depth) with an average rate of ∼14 yr cm^{-1}, the soil bulk density remains constant at 4041−4506 g m^{-2} cm^{-1} (mean = 4390 g m^{-2} cm^{-1}). In this layer, soil Hg concentration increases with soil depth from 112 ± 1 (11 cm) to 145 ± 1 ng g^{-1} (15 cm), enhancing the soil Hg pool from 490 to 653 μg m^{-2} cm^{-1}. Different from the steadily positive shift (up to +0.48‰) of δ^{202}Hg in stages A−C, the δ^{202}Hg and Δ^{199}Hg signatures remain nearly constant at −1.81‰ to −1.83‰ for δ^{202}Hg and −0.64‰ and −0.69‰ for Δ^{199}Hg in stage D.

Since Hg MDF occurs nearly universally in transformational and transitional processes[16,35] and heavier isotopes are preferentially remained in the residual soil, the relatively stable MDF in this soil layer indicates limited Hg transformation. Given the absence of immediate Hg sources, the increased Hg concentration in the deeper organic soil is likely due to the further loss of organic carbon mass. This is supported by the deceasing C (from 7.5% to 6.4%) content and increasing of Hg/C ratio (from 1.2 to 2.3), as shown in Figure 6.

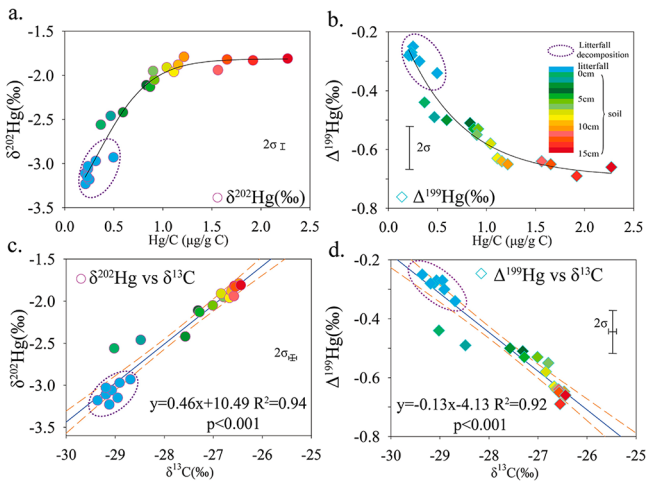

Figure 6. Ratios of (a) Hg/C versus δ^{202}Hg, (b) Hg/C versus Δ^{199}Hg, (c) δ^{13}C versus δ^{202}Hg, and (d) δ^{13}C versus Δ^{199}Hg from the litterfall degradation to deep organic soil. The regression lines are based on all samples, including the litterfall and soil samples. Measured error bar represents ±2 standard deviation.

Conversion of thiol-bound Hg^{II} to nanoparticulate β-HgS under ambient conditions can occur in natural organic matter, and at least 90% of the Hg stored in the Ah soil horizon is precipitated as nanoparticulate metacinnabar (β-HgS_{NP}).[60,66] Therefore, it is possible that that Hg is immobilized and accumulates in the macromolecules or reprecipitated as nano β-HgS.

3.5. Modeling Uncertainties. There are additional processes contributing to the observed isotopic shift, but they were not included in the modeling because of existing knowledge gaps. The atmospheric Hg deposition flux treated in the model can only rely on the measurements made in the last decades at the study site (∼30 μg m^{-2} yr^{-1} throughfall deposition and ∼75 μg m^{-2} yr^{-1} litterfall deposition).[10,43] Uncertainties in wet and dry deposition over the past 500 year period could be variable due to the changes in climate, vegetative development, and Hg emissions, causing immeasurable impact on our model results, especially in stage C with 420 years of decomposition. Another factor not considered in the model is the Hg loss through runoff and infiltration flows. It is known that Hg is bound to NOM in forest runoff.[52] Although Hg^{II} carried away by runoff is of small quantity on an annual basis,[53] the total cumulative loss via runoff over the 500 year period should not be ignored. Also not considered in the model is the dynamic bidirectional air−soil exchange of Hg^0,[67,68] which may be another direct Hg^0 input to forest floor. The porous nature of the litter layer and its high organic content can facilitate sorption of Hg^0 vapor and store the Hg uptake with the reduced sulfur functional groups in humic substances.[5,10,69] The lack of understanding in Hg^0 sorption by soil (direct Hg^0 input) and dark oxidation by NOM also limits model parametrization for these processes that are not well understood. The observed level of Hg isotopic fractionation caused by Hg^0 sorption and dark oxidation by NOM on forest floor is diverse. Under designed laboratory conditions, Zheng et. al[32] suggested two possible mechanisms: One is the oxidation of Hg^0 to Hg^{2+} caused by thiols with the kinetic isotope effect (KIE), and the other is the equilibrium isotope effect (EIE) between thiol-bound Hg^{2+} and residual Hg^0 vapor.[32] The overall Hg isotopic fractionations are predominantly caused by EIE, leading to enrichment factors for MDF and MIF ($\varepsilon^{202}Hg_{P/R}$ and E^{199}Hg) ranging from 1.10‰ to 1.56‰ and from −0.16‰ to −0.18‰.[32] Given the multiple mathematical constrains of the unknown processes, an exact model solution is not possible, which is a limitation of the modeling work.

A two-level factorial modeling experiment and a Monte Carlo simulation were performed to quantify the uncertainties caused by the model parameters (Figures S7−S12, Tables S4 and S5, and Section 4 in the SI). In the two-level factorial modeling experiment, a main effect is the mean effect of one independent variable on the response, and two-way interaction effect is the combined effect compared to the sum of two main effects for determining synergistic or antagonistic effect of two factors on the response. Figures S7−S9 show that precipitation Hg input is the predominant factor in shifting the contribution of various reduction pathways during stages A and B. On average, an increase in precipitation Hg input from 2% to 8% significantly increases the fractional contribution of microbial reduction by 3%−11%, organosulfur photoreduction by −1% to +8%, DOM photoreduction by −1% to +0.5%, and NOM dark reduction by −17% to −2%. The isotope enrichment factor of NOM dark reduction also plays an important role in shifting its process contribution, resulting in ±3% of variability in stages A and B and up to ±15% in stage C. Other main and interaction effects among Hg isotope enrichment factors are relatively weak (∼3% or below). Overall, the generally low main and interaction effects among Hg isotope enrichment factors indicate independence of each reduction process in soil.

The Monte Carlo simulation further confirms that the Hg isotopic fractionation model results depend primarily on the assumed Hg input from precipitation (Figures S10−S12). With a given precipitation Hg input, the results of Monte Carlo simulation fall within a narrow range (±10%) of estimated means of Hg isotopic fractionation factors. This suggests that variations of Hg isotope enrichment factors in the mixing model does not significantly influence the model results.

3.6. Relationship between Hg, C, and Its Isotopic Transition. The C/N ratio is a useful metric for estimating the degree of vegetative biomass decomposition. A higher C/N ratio is found in fresh foliage, while a lower C/N ratio is indicative of decomposed biomass and soil.[70,71] The C/N ratios gradually decrease from 45 (surface layer) to 15 (at 15

https://dx.doi.org/10.1021/acs.est.0c00950
Environ. Sci. Technol. 2020, 54, 8739−8749

cm depth) over the 500 year period (Figure S3). Since a large fraction of Hg^{II} is retained in soil through complex formation with soil organic matter (SOM),[52] the Hg/C ratio also increases with the soil age and depth (Figure 6a,b). Obrist et al.[72] attributed such increases to two reasons. One is that Hg accumulation due to sorption may be more important than "internal" accumulation. The other is selective Hg sorption to different organic matter fraction in the decomposing process.

Interestingly, the observed Hg MDF (δ^{202}Hg) increases with the Hg/C ratio until approaching a value of ~−1.8‰ at Hg/C of 1.2 (Figure 6a) and then stays relatively constant from Hg/C of 1.2−1.8. Similarly, Hg odd-MIF (Δ^{199}Hg) decreases with increasing Hg/C until Hg/C > 1.2 and then stabilizes (Figure 6b). A Hg/C ratio >1.2 is found in stage D, indicating that Hg is complexed with aged organic matter[72] and remains stable as discussed in Section 3.4. The δ^{13}C correlates consistently with δ^{202}Hg (R^2 = 0.94) and Δ^{199}Hg (R^2 = 0.92) in this organic soil profile (Figure 6c,d), reinforcing the hypothesis that Hg reduction during litter humification can cause kinetic MDF and odd-MIF in correlation with δ^{13}C values. The microbiologically mediated NOM decomposition is the primary cause for the isotope fractionations of C on forest floor.[73,74] Decomposition of NOM possibly releases the absorbed Hg that is subsequently subject to reduction-induced Hg isotopic fractionation driven by sunlight, microbes, and organic matters. The strong correlation between Hg and C isotopes supports the global geospatial distribution of Hg storage in soil reported earlier[8,72,75] and implies that the fate of Hg in aging soil is closely linked to soil organic matters.

4. IMPLICATIONS

A large amount of Hg is sequestered in vegetated surface soil globally (0−20 cm, 1088 ± 379 Gg).[8] Thirty-two percent of the surface Hg resides in tropical/subtropical forest where Hg biogeochemical cycling is particularly active due to the moderate temperature and abundant rainfall.[8] Approximately 70% of global Hg^0 dry deposition through litterfall (1000−1200 Mg yr^{-1}) occurs in the tropical and subtropical regions due to the rapid biomass production.[2,3] In this study, we demonstrated that the compositions of stable Hg and C isotopes reflect the transformation and sequestration processes of Hg contained in litters and soil on the forest floor of subtropical evergreen broad-leaf forest ecosystem. Our findings indicate that microbial reduction and photoreduction are the predominant processes shifting Hg isotopic composition in the first 20 years decomposition period, after which organic matter dark reduction continues to modify Hg isotope signatures. It is likely that Hg reduction under dark conditions driven by NVE is ubiquitous in forest organic soil, which has been observed in boreal forests,[7] tropical forests,[13] and now in subtropical evergreen forests. Although the abiotic reduction by NOM has been included in a global box model,[18] we recommend the process be incorporated in comprehensive chemical transport models, such as GEOS-Chem.[70,76] Hg in the deeper organic soil layer is unlikely to participate in the air−soil exchange process in the subtropical forest ecosystem. Hence, the large inert Hg reservoir in the deeper layer of organic soil (soil depth depending on sites) should also be considered in optimizing current Hg global cycle models.

■ ASSOCIATED CONTENT

Supporting Information

The Supporting Information is available free of charge at https://pubs.acs.org/doi/10.1021/acs.est.0c00950.

Discussions of soil sampling description, Hg isotope measurements, quality assurance and control, Hg isotopic fractionation model, sensitivity analysis, and R programming language codes for stages A−C, tables of litterfall mass, C and N content, and C isotope composition, Hg concentration and isotope compositions, C and Hg isotope compositions, examined model variables and the experimental levels of factorial design, and isotopic enrichment factors of reductive pathways, and figures of study area and selected sampling locations schematics, soil profiles, soil Hg concentration, variations of dry soil mass unit area and C/N ratio with the increasing soil depth, estimated contributions by different potential processes during decomposition, Δ^{199}Hg versus δ^{202}Hg plots, ratio of Δ^{199}Hg/Δ^{201}Hg versus soil depth, sensitivity analyses, and estimates of Monte Carlo simulation (PDF)

■ AUTHOR INFORMATION

Corresponding Author

Xinbin Feng − *State Key Laboratory of Environmental Geochemistry, Institute of Geochemistry, Chinese Academy of Sciences, Guiyang 550081, China; Center for Excellence in Quaternary Science and Global Change, Chinese Academy of Sciences, Xian 710061, China;* orcid.org/0000-0002-7462-8998; Phone: +86-851-85895728; Email: fengxinbin@vip.skleg.cn

Authors

Wei Yuan − *State Key Laboratory of Environmental Geochemistry, Institute of Geochemistry, Chinese Academy of Sciences, Guiyang 550081, China; University of Chinese Academy of Sciences, Beijing 100049, China*

Xun Wang − *College of Resources and Environment, Southwest University, Chongqing 400715, China;* orcid.org/0000-0002-7407-8965

Che-Jen Lin − *Center for Advances in Water and Air Quality, Lamar University, Beaumont, Texas 77710, United States*

Chuansheng Wu − *Anhui Province Key Laboratory of Environmental Hormone and Reproduction, Fuyang Normal University, Anhui 236037, China*

Leiming Zhang − *Air Quality Research Division, Science and Technology Branch, Environment and Climate Change Canada, Toronto, Ontario M3H 5T4, Canada;* orcid.org/0000-0001-5437-5412

Bo Wang − *State Key Laboratory of Environmental Geochemistry, Institute of Geochemistry, Chinese Academy of Sciences, Guiyang 550081, China; University of Chinese Academy of Sciences, Beijing 100049, China*

Jonas Sommar − *State Key Laboratory of Environmental Geochemistry, Institute of Geochemistry, Chinese Academy of Sciences, Guiyang 550081, China*

Zhiyun Lu − *National Forest Ecosystem Research Station at Ailaoshan, Yunnan 676209, China*

Complete contact information is available at: https://pubs.acs.org/10.1021/acs.est.0c00950

https://dx.doi.org/10.1021/acs.est.0c00950
Environ. Sci. Technol. 2020, 54, 8739−8749

Notes

The authors declare no competing financial interest.

■ ACKNOWLEDGMENTS

This work was funded by the National Natural Science Foundation of China (41430754, 41829701, 41703134, 41921004), Strategic Priority Research Programs of the Chinese Academy of Sciences, the Pan-Third Pole Environment Study for a Green Silk Road (Pan-TPE, XDA2004050201), and K. C. Wong Education Foundation. The data used in this study are tabulated in the SI.

■ REFERENCES

(1) Fu, X. W.; Zhu, W.; Zhang, H.; Sommar, J.; Yu, B.; Yang, X.; Wang, X.; Lin, C. J.; Feng, X. B. Depletion of atmospheric gaseous elemental mercury by plant uptake at Mt. Changbai, Northeast China. *Atmos. Chem. Phys.* **2016**, *16* (20), 12861−12873.

(2) Wang, X.; Bao, Z.; Lin, C.-J.; Yuan, W.; Feng, X. Assessment of Global Mercury Deposition through Litterfall. *Environ. Sci. Technol.* **2016**, *50* (16), 8548−8557.

(3) Obrist, D. Atmospheric mercury pollution due to losses of terrestrial carbon pools? *Biogeochemistry* **2007**, *85* (2), 119−123.

(4) Lindberg, S.; Bullock, R.; Ebinghaus, R.; Engstrom, D.; Feng, X. B.; Fitzgerald, W.; Pirrone, N.; Prestbo, E.; Seigneur, C. A synthesis of progress and uncertainties in attributing the sources of mercury in deposition. *Ambio* **2007**, *36* (1), 19−32.

(5) Zheng, W.; Obrist, D.; Weis, D.; Bergquist, B. A. Mercury isotope compositions across North American forests. *Global Biogeochem Cy* **2016**, *30* (10), 1475−1492.

(6) Wang, X.; Luo, J.; Yin, R.; Yuan, W.; Lin, C.-J.; Sommar, J.; Feng, X.; Wang, H.; Lin, C. Using Mercury Isotopes To Understand Mercury Accumulation in the Montane Forest Floor of the Eastern Tibetan Plateau. *Environ. Sci. Technol.* **2017**, *51* (2), 801−809.

(7) Jiskra, M.; Wiederhold, J. G.; Skyllberg, U.; Kronberg, R.-M.; Hajdas, I.; Kretzschmar, R. Mercury Deposition and Re-emission Pathways in Boreal Forest Soils Investigated with Hg Isotope Signatures. *Environ. Sci. Technol.* **2015**, *49* (12), 7188−7196.

(8) Wang, X.; Yuan, W.; Lin, C.-J.; Zhang, L.; Zhang, H.; Feng, X. Climate and Vegetation As Primary Drivers for Global Mercury Storage in Surface Soil. *Environ. Sci. Technol.* **2019**, *53* (18), 10665−10675.

(9) Whitehead, D. Forests as carbon sinks—benefits and consequences. *Tree Physiol.* **2011**, *31* (9), 893−902.

(10) Wang, X.; Lin, C. J.; Lu, Z. Y.; Zhang, H.; Zhang, Y. P.; Feng, X. B. Enhanced accumulation and storage of mercury on subtropical evergreen forest floor: Implications on mercury budget in global forest ecosystems. *J. Geophys. Res.: Biogeosci.* **2016**, *121* (8), 2096−2109.

(11) Gu, B.; Bian, Y.; Miller, C. L.; Dong, W.; Jiang, X.; Liang, L. Mercury reduction and complexation by natural organic matter in anoxic environments. *Proc. Natl. Acad. Sci. U. S. A.* **2011**, *108* (4), 1479−1483.

(12) Zheng, W.; Liang, L.; Gu, B. Mercury Reduction and Oxidation by Reduced Natural Organic Matter in Anoxic Environments. *Environ. Sci. Technol.* **2012**, *46* (1), 292−299.

(13) Guédron, S.; Amouroux, D.; Tessier, E.; Grimaldi, C.; Barre, J.; Berail, S.; Perrot, V.; Grimaldi, M. Mercury Isotopic Fractionation during Pedogenesis in a Tropical Forest Soil Catena (French Guiana): Deciphering the Impact of Historical Gold Mining. *Environ. Sci. Technol.* **2018**, *52* (20), 11573−11582.

(14) Mazur, M. E. E.; Eckley, C. S.; Mitchell, C. P. J. Susceptibility of Soil Bound Mercury to Gaseous Emission As a Function of Source Depth: An Enriched Isotope Tracer Investigation. *Environ. Sci. Technol.* **2015**, *49* (15), 9143−9149.

(15) Obrist, D.; Pokharel, A. K.; Moore, C. Vertical Profile Measurements of Soil Air Suggest Immobilization of Gaseous Elemental Mercury in Mineral Soil. *Environ. Sci. Technol.* **2014**, *48* (4), 2242−2252.

(16) Blum, J. D.; Sherman, L. S.; Johnson, M. W. Mercury Isotopes in Earth and Environmental Sciences. *Annu. Rev. Earth Pl Sc* **2014**, *42* (1), 249−269.

(17) Bergquist, R. A.; Blum, J. D. The Odds and Evens of Mercury Isotopes: Applications of Mass-Dependent and Mass-Independent Isotope Fractionation. *Elements* **2009**, *5* (6), 353−357.

(18) Sun, R. Y.; Jiskra, M.; Amos, H. M.; Zhang, Y. X.; Sunderland, E. M.; Sonke, J. E. Modelling the mercury stable isotope distribution of Earth surface reservoirs: Implications for global Hg cycling. *Geochim. Cosmochim. Acta* **2019**, *246*, 156−173.

(19) Tsui, M. T.-K.; Blum, J. D.; Kwon, S. Y. Review of stable mercury isotopes in ecology and biogeochemistry. *Sci. Total Environ.* **2020**, *716*, 135386.

(20) Kritee, K.; Blum, J. D.; Barkay, T. Mercury Stable Isotope Fractionation during Reduction of Hg(II) by Different Microbial Pathways. *Environ. Sci. Technol.* **2008**, *42* (24), 9171−9177.

(21) Kritee, K.; Blum, J. D.; Johnson, M. W.; Bergquist, B. A.; Barkay, T. Mercury stable isotope fractionation during reduction of Hg(II) to Hg(0) by mercury resistant microorganisms. *Environ. Sci. Technol.* **2007**, *41* (6), 1889−1895.

(22) Kwon, S. Y.; Blum, J. D.; Yin, R.; Tsui, M. T.-K.; Yang, Y. H.; Choi, J. W. Mercury stable isotopes for monitoring the effectiveness of the Minamata Convention on Mercury. *Earth-Sci. Rev.* **2020**, *203*, 103111.

(23) Estrade, N.; Carignan, J.; Sonke, J. E.; Donard, O. F. X. Mercury isotope fractionation during liquid-vapor evaporation experiments. *Geochim. Cosmochim. Acta* **2009**, *73* (10), 2693−2711.

(24) Wiederhold, J. G.; Cramer, C. J.; Daniel, K.; Infante, I.; Bourdon, B.; Kretzschmar, R. Equilibrium Mercury Isotope Fractionation between Dissolved Hg(II) Species and Thiol-Bound Hg. *Environ. Sci. Technol.* **2010**, *44* (11), 4191−4197.

(25) Bergquist, B. A.; Blum, J. D. Mass-dependent and -independent fractionation of Hg isotopes by photoreduction in aquatic systems. *Science* **2007**, *318* (5849), 417−420.

(26) Zheng, W.; Hintelmann, H. Mercury isotope fractionation during photoreduction in natural water is controlled by its Hg/DOC ratio. *Geochim. Cosmochim. Acta* **2009**, *73* (22), 6704−6715.

(27) Zheng, W.; Hintelmann, H. Isotope Fractionation of Mercury during Its Photochemical Reduction by Low-Molecular-Weight Organic Compounds. *J. Phys. Chem. A* **2010**, *114* (12), 4246−4253.

(28) Sherman, L. S.; Blum, J. D.; Johnson, K. P.; Keeler, G. J.; Barres, J. A.; Douglas, T. A. Mass-independent fractionation of mercury isotopes in Arctic snow driven by sunlight. *Nat. Geosci.* **2010**, *3* (3), 173−177.

(29) Kritee, K.; Motta, L. C.; Blum, J. D.; Tsui, M. T.-K.; Reinfelder, J. R. Photomicrobial Visible Light-Induced Magnetic Mass Independent Fractionation of Mercury in a Marine Microalga. *ACS Earth and Space Chemistry* **2018**, *2* (5), 432−440.

(30) Ghosh, S.; Schauble, E. A.; Couloume, G. L.; Blum, J. D.; Bergquist, B. A. Estimation of nuclear volume dependent fractionation of mercury isotopes in equilibrium liquid-vapor evaporation experiments. *Chem. Geol.* **2013**, *336*, 5−12.

(31) Zheng, W.; Hintelmann, H. Nuclear Field Shift Effect in Isotope Fractionation of Mercury during Abiotic Reduction in the Absence of Light. *J. Phys. Chem. A* **2010**, *114* (12), 4238−4245.

(32) Zheng, W.; Demers, J. D.; Lu, X.; Bergquist, B. A.; Anbar, A. D.; Blum, J. D.; Gu, B. Mercury Stable Isotope Fractionation during Abiotic Dark Oxidation in the Presence of Thiols and Natural Organic Matter. *Environ. Sci. Technol.* **2019**, *53* (4), 1853−1862.

(33) Sun, G. Y.; Sommar, J.; Feng, X. B.; Lin, C. J.; Ge, M. F.; Wang, W. G.; Yin, R. S.; Fu, X. W.; Shang, L. H. Mass-Dependent and -Independent Fractionation of Mercury Isotope during Gas-Phase Oxidation of Elemental Mercury Vapor by Atomic Cl and Br. *Environ. Sci. Technol.* **2016**, *50* (17), 9232−9241.

(34) Mead, C.; Lyons, J. R.; Johnson, T. M.; Anbar, A. D. Unique Hg Stable Isotope Signatures of Compact Fluorescent Lamp-Sourced Hg. *Environ. Sci. Technol.* **2013**, *47* (6), 2542−2547.

(35) Blum, J. D.; Johnson, M. W. Recent Developments in Mercury Stable Isotope Analysis. *Rev. Mineral. Geochem.* **2017**, *82*, 733−757.

https://dx.doi.org/10.1021/acs.est.0c00950
Environ. Sci. Technol. 2020, 54, 8739−8749

(36) Demers, J. D.; Blum, J. D.; Zak, D. R. Mercury isotopes in a forested ecosystem: Implications for air-surface exchange dynamics and the global mercury cycle. *Global Biogeochem Cy* **2013**, *27* (1), 222−238.
(37) Chen, J. B.; Hintelmann, H.; Feng, X. B.; Dimock, B. Unusual fractionation of both odd and even mercury isotopes in precipitation from Peterborough, ON, Canada. *Geochim. Cosmochim. Acta* **2012**, *90*, 33−46.
(38) Smith, C. N.; Kesler, S. E.; Blum, J. D.; Rytuba, J. J. Isotope geochemistry of mercury in source rocks, mineral deposits and spring deposits of the California Coast Ranges, USA. *Earth Planet. Sci. Lett.* **2008**, *269* (3), 399−407.
(39) Wang, X.; Luo, J.; Yuan, W.; Lin, C.-J.; Wang, F.; Liu, C.; Wang, G.; Feng, X. Global warming accelerates uptake of atmospheric mercury in regions experiencing glacier retreat. *Proc. Natl. Acad. Sci. U. S. A.* **2020**, *117*, 2049−2055.
(40) Obrist, D.; Agnan, Y.; Jiskra, M.; Olson, C. L.; Colegrove, D. P.; Hueber, J.; Moore, C. W.; Sonke, J. E.; Helmig, D. Tundra uptake of atmospheric elemental mercury drives Arctic mercury pollution. *Nature* **2017**, *547* (7662), 201−204.
(41) Tan, Z. H.; Zhang, Y. P.; Schaefer, D.; Yu, G. R.; Liang, N.; Song, Q. H. An old-growth subtropical Asian evergreen forest as a large carbon sink. *Atmos. Environ.* **2011**, *45* (8), 1548−1554.
(42) Yuan, W.; Sommar, J.; Lin, C.-J.; Wang, X.; Li, K.; Liu, Y.; Zhang, H.; Lu, Z.; Wu, C.; Feng, X. Stable Isotope Evidence Shows Re-emission of Elemental Mercury Vapor Occurring after Reductive Loss from Foliage. *Environ. Sci. Technol.* **2019**, *53* (2), 651−660.
(43) Zhou, J.; Feng, X.; Liu, H.; Zhang, H.; Fu, X.; Bao, Z.; Wang, X.; Zhang, Y. Examination of total mercury inputs by precipitation and litterfall in a remote upland forest of Southwestern China. *Atmos. Environ.* **2013**, *81*, 364−372.
(44) Ribeiro, C.; Madeira, M.; Araújo, M. C. Decomposition and nutrient release from leaf litter of Eucalyptus globulus grown under different water and nutrient regimes. *For. Ecol. Manage.* **2002**, *171* (1), 31−41.
(45) Pokharel, A. K.; Obrist, D. Fate of mercury in tree litter during decomposition. *Biogeosciences* **2011**, *8* (9), 2507−2521.
(46) Blum, J. D.; Bergquist, B. A. Reporting of variations in the natural isotopic composition of mercury. *Anal. Bioanal. Chem.* **2007**, *388* (2), 353−359.
(47) Estrade, N.; Carignan, J.; Sonke, J. E.; Donard, O. F. X. Measuring Hg Isotopes in Bio-Geo-Environmental Reference Materials. *Geostand. Geoanal. Res.* **2010**, *34* (1), 79−93.
(48) Radke, J.; Deerberg, M.; Hilkert, A.; Schlüter, H. J.; Schwieters, J. High Resolution Double-Focusing Isotope Ratio Mass Spectrometry. *Geophysical Research Abstracts* **2012**, *14* (23), 12549.
(49) Reimer, P. J.; Bard, E.; Bayliss, A.; Beck, J. W.; Blackwell, P. G.; Ramsey, C. B.; Buck, C. E.; Cheng, H.; Edwards, R. L.; Friedrich, M.; Grootes, P. M.; Guilderson, T. P.; Haflidason, H.; Hajdas, I.; Hatté, C.; Heaton, T. J.; Hoffmann, D. L.; Hogg, A. G.; Hughen, K. A.; Kaiser, K. F.; Kromer, B.; Manning, S. W.; Niu, M.; Reimer, R. W.; Richards, D. A.; Scott, E. M.; Southon, J. R.; Staff, R. A.; Turney, C. S. M.; van der Plicht, J. IntCal13 and Marine13 Radiocarbon Age Calibration Curves 0−50,000 Years cal BP. *Radiocarbon* **2013**, *55* (4), 1869−1887.
(50) Hua, Q.; Barbetti, M.; Rakowski, A. Z. Atmospheric Radiocarbon for the Period 1950−2010. *Radiocarbon* **2013**, *55* (4), 2059−2072.
(51) Blaauw, M.; Christen, J. A. Flexible paleoclimate age-depth models using an autoregressive gamma process. *Bayesian Anal.* **2011**, *6* (3), 457−474.
(52) Jiskra, M.; Wiederhold, J. G.; Skyllberg, U.; Kronberg, R. M.; Kretzschmar, R. Source tracing of natural organic matter bound mercury in boreal forest runoff with mercury stable isotopes. *Environmental Science Processes & Impacts* **2017**, *19* (10), 1235.
(53) Woerndle, G. E.; Tsui, M. T. K.; Sebestyen, S. D.; Blum, J. D.; Nie, X. P.; Kolka, R. K. New Insights on Ecosystem Mercury Cycling Revealed by Stable Isotopes of Mercury in Water Flowing from a Headwater Peatland Catchment. *Environ. Sci. Technol.* **2018**, *52* (4), 1854−1861.
(54) Blum, J. D.; Anbar, A. D. Mercury isotopes in the late Archean Mount McRae Shale. *Geochim Cosmochim Ac* **2010**, *74* (12), A98−A98.
(55) Li, K.; Lin, C.-J.; Yuan, W.; Sun, G.; Fu, X.; Feng, X. An improved method for recovering and preconcentrating mercury in natural water samples for stable isotope analysis. *J. Anal. At. Spectrom.* **2019**, *34* (11), 2303−2313.
(56) Zhang, H.; Fu, X.; Lin, C. J.; Shang, L.; Zhang, Y.; Feng, X.; Lin, C. Monsoon-facilitated characteristics and transport of atmospheric mercury at a high-altitude background site in southwestern China. *Atmos. Chem. Phys.* **2016**, *16* (20), 13131−13148.
(57) Connin, S. L.; Feng, X.; Virginia, R. A. Isotopic discrimination during long-term decomposition in an arid land ecosystem. *Soil Biol. Biochem.* **2001**, *33* (1), 41−51.
(58) Gioacchini, P.; Masia, A.; Canaccini, F.; Boldreghini, P.; Tonon, G. Isotopic discrimination during litter decomposition and δ13C and δ15N soil profiles in a young artificial stand and in an old floodplain forest. *Isot. Environ. Health Stud.* **2006**, *42* (2), 135−149.
(59) Feng, X. A theoretical analysis of carbon isotope evolution of decomposing plant litters and soil organic matter. *Global Biogeochem Cy* **2002**, *16* (4), 66-1−66-11.
(60) Manceau, A.; Wang, J.; Rovezzi, M.; Glatzel, P.; Feng, X. Biogenesis of Mercury-Sulfur Nanoparticles in Plant Leaves from Atmospheric Gaseous Mercury. *Environ. Sci. Technol.* **2018**, *52* (7), 3935.
(61) Gratz, L. E.; Keeler, G. J.; Blum, J. D.; Sherman, L. S. Isotopic Composition and Fractionation of Mercury in Great Lakes Precipitation and Ambient Air. *Environ. Sci. Technol.* **2010**, *44* (20), 7764−7770.
(62) Donovan, P. M.; Blum, J. D.; Yee, D.; Gehrke, G. E.; Singer, M. B. An isotopic record of mercury in San Francisco Bay sediment. *Chem. Geol.* **2013**, *349*, 87−98.
(63) Yuan, W.; Wang, X.; Lin, C.-J.; Sommar, J.; Lu, Z.; Feng, X. Process factors driving dynamic exchange of elemental mercury vapor over soil in broadleaf forest ecosystems. *Atmos. Environ.* **2019**, *219*, 117047.
(64) Yu, B.; Fu, X. W.; Yin, R. S.; Zhang, H.; Wang, X.; Lin, C. J.; Wu, C. S.; Zhang, Y. P.; He, N. N.; Fu, P. Q.; Wang, Z. F.; Shang, L. H.; Sommar, J.; Sonke, J. E.; Maurice, L.; Guinot, B.; Feng, X. B. Isotopic Composition of Atmospheric Mercury in China: New Evidence for Sources and Transformation Processes in Air and in Vegetation. *Environ. Sci. Technol.* **2016**, *50* (17), 9262−9269.
(65) Cantrell, C. A. Technical Note: Review of methods for linear least-squares fitting of data and application to atmospheric chemistry problems. *Atmos. Chem. Phys.* **2008**, *8* (17), 5477−5487.
(66) Manceau, A.; Lemouchi, C.; Enescu, M.; Gaillot, A.-C.; Lanson, M.; Magnin, V.; Glatzel, P.; Poulin, B. A.; Ryan, J. N.; Aiken, G. R.; Gautier-Luneau, I.; Nagy, K. L. Formation of Mercury Sulfide from Hg(II)−Thiolate Complexes in Natural Organic Matter. *Environ. Sci. Technol.* **2015**, *49* (16), 9787−9796.
(67) Zhu, W.; Lin, C. J.; Wang, X.; Sommar, J.; Fu, X. W.; Feng, X. B. Global observations and modeling of atmosphere-surface exchange of elemental mercury: a critical review. *Atmos. Chem. Phys.* **2016**, *16* (7), 4451−4480.
(68) Agnan, Y.; Le Dantec, T.; Moore, C. W.; Edwards, G. C.; Obrist, D. New Constraints on Terrestrial Surface Atmosphere Fluxes of Gaseous Elemental Mercury Using a Global Database. *Environ. Sci. Technol.* **2016**, *50* (2), 507−524.
(69) Jiskra, M.; Sonke, J. E.; Agnan, Y.; Helmig, D.; Obrist, D. Insights from mercury stable isotopes on terrestrial-atmosphere exchange of Hg(0) in the Arctic tundra. *Biogeosciences* **2019**, *16* (20), 4051−4064.
(70) Smith-Downey, N. V.; Sunderland, E. M.; Jacob, D. J. Anthropogenic impacts on global storage and emissions of mercury from terrestrial soils: Insights from a new global model. *J. Geophys. Res.* **2010**, *115*, 115.

https://dx.doi.org/10.1021/acs.est.0c00950
Environ. Sci. Technol. 2020, 54, 8739−8749

(71) Obrist, D.; Tas, E.; Peleg, M.; Matveev, V.; Fain, X.; Asaf, D.; Luria, M. Bromine-induced oxidation of mercury in the mid-latitude atmosphere. *Nat. Geosci.* **2011**, *4* (1), 22−26.
(72) Obrist, D.; Johnson, D. W.; Lindberg, S. E.; Luo, Y.; Hararuk, O.; Bracho, R.; Battles, J. J.; Dail, D. B.; Edmonds, R. L.; Monson, R. K.; Ollinger, S. V.; Pallardy, S. G.; Pregitzer, K. S.; Todd, D. E. Mercury Distribution Across 14 US Forests. Part I: Spatial Patterns of Concentrations in Biomass, Litter, and Soils. *Environ. Sci. Technol.* **2011**, *45* (9), 3974−3981.
(73) Hobbie, E. A.; Ouimette, A. P. Controls of Nitrogen Isotope Patterns in Soil Profiles. *Biogeochemistry* **2009**, *95*, 355−371.
(74) Natelhoffer, K. J.; Fry, B. *Controls on Natural Nitrogen-15 and Carbon-13 Abundances in Forest Soil Organic Matter.* **1988**, *52* (6), 1633−1640.
(75) Schuster, P. F.; Schaefer, K. M.; Aiken, G. R.; Antweiler, R. C.; Dewild, J. F.; Gryziec, J. D.; Gusmeroli, A.; Hugelius, G.; Jafarov, E.; Krabbenhoft, D. P.; Liu, L.; Herman-Mercer, N.; Mu, C.; Roth, D. A.; Schaefer, T.; Striegl, R. G.; Wickland, K. P.; Zhang, T. Permafrost Stores a Globally Significant Amount of Mercury. *Geophys. Res. Lett.* **2018**, *45* (3), 1463−1471.
(76) Amos, H. M.; Jacob, D. J.; Streets, D. G.; Sunderland, E. M. Legacy impacts of all-time anthropogenic emissions on the global mercury cycle. *Global Biogeochem Cy* **2013**, *27* (2), 410−421.

https://dx.doi.org/10.1021/acs.est.0c00950
Environ. Sci. Technol. 2020, 54, 8739−8749